Editors' Suggestion

# Design, fabrication, and high-gradient testing of an *X*-band, traveling-wave accelerating structure milled from copper halves

Theodoros Argyropoulos, Nuria Catalan-Lasheras, Alexej Grudiev, Gerard Mcmonagle, Enrique Rodriguez-Castro, Igor Syrachev, Rolf Wegner, Ben Woolley, Walter Wuensch, and Hao Zha
*European Organisation for Nuclear Research (CERN), 1211 Geneva, Switzerland*

Valery Dolgashev, Gorden Bowden, and Andrew Haase
*SLAC, Menlo Park, California 94025, USA*

Thomas Geoffrey Lucas* and Matteo Volpi
*University of Melbourne, Parkville 3010, Australia*

Daniel Esperante-Pereira
*Instituto de Fisica Corpuscular (IFIC), Valencia, Spain*

Robin Rajamäki
*Aalto University, 02150 Espoo, Finland*

(Received 9 February 2018; published 7 June 2018)

A prototype 11.994 GHz, traveling-wave accelerating structure for the Compact Linear Collider has been built, using the novel technique of assembling the structure from milled halves. The use of milled halves has many advantages when compared to a structure made from individual disks. These include the potential for a reduction in cost, because there are fewer parts, as well as a greater freedom in choice of joining technology because there are no rf currents across the halves' joint. Here we present the rf design and fabrication of the prototype structure, followed by the results of the high-power test and post-test surface analysis. During high-power testing the structure reached an unloaded gradient of 100 MV/m at a rf breakdown rate of less than $1.5 \times 10^{-5}$ breakdowns/pulse/m with a 200 ns pulse. This structure has been designed for the CLIC testing program but construction from halves can be advantageous in a wide variety of applications.

DOI: 10.1103/PhysRevAccelBeams.21.061001

## I. INTRODUCTION

In order to optimize the performance and cost of the Compact Linear Collider (CLIC), a significant effort is being placed into the development of high gradient normal conducting accelerating structures. The structures for CLIC are designed to operate at 11.994 GHz with an unloaded accelerating gradient of 100 MV/m, an rf pulse length of 240 ns with a 180 ns flat-top, and a breakdown rate (BDR) lower than $3 \times 10^{-7}$ breakdowns/pulse/m. Fabricated from copper, the structures are manufactured through a combination of precision turning and milling of the individual accelerating cell disks. The numerous individual disks in CLIC structures are generally joined together through diffusion bonding [1,2].

Here we introduce an alternative approach to assembling the structure from individual disks. The novel technique uses precision milling to fabricate structure halves from copper blocks. This accelerating structure design builds upon previous work of an accelerating structure made from quadrants [3], as well as the power extraction and transfer structures for CLIC's drive beam which are constructed from octants [1]. The new assembly method gives a number of advantages compared to traditional disk-based structures, providing the motivation for this study. Particularly notable are: a reduction of the number of precision pieces, freedom of choice in joining technology since there are no rf currents flowing through the metal-to-metal joint, the use of unique geometry for higher order mode damping, the ability to perform bead-pulling

*Corresponding author.
thomas.geoffrey.lucas@cern.ch

measurements before brazing, and an overall reduction of the total manufacturing cost [4].

In this paper we present the rf design and fabrication of the structure, followed by the high-power testing and post-test analysis. Known as CLIC-G-Open, the tapered (constant gradient), traveling-wave structure consists of 24 regular cells and 2 matching cells for the input and output couplers. This design was based on the CLIC-G (T24) which had been tested at high gradients and low breakdown rate [1]. Mechanical design and fabrication was undertaken at SLAC after which the structure was shipped to CERN for high power testing where the structure was installed on CERN's X-band Test Stand, Xbox-2 [5].

## II. REGULAR CELL GEOMETRY

The starting point of the structure began with the well tested CLIC-G structure design which operates with 120° phase advance per cell [1]. Figure 1 illustrates the introduction of a gap between the two halves of the structure to avoid unbrazed metal-to-metal contacts. The 1 mm gap is cut off at the working frequency to minimize fields leaking towards brazed surfaces and thus reducing the effects of imperfections of brazing fillets on

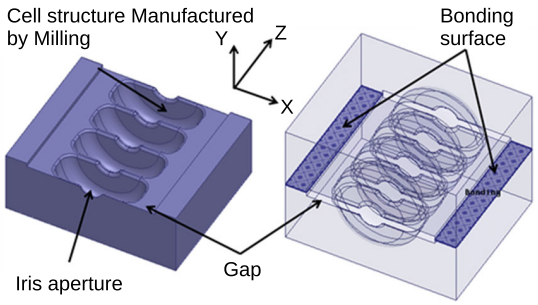


FIG. 1. The HFSS design of the structure demonstrating the structure half on the left and how each half will be joined together [7,9].

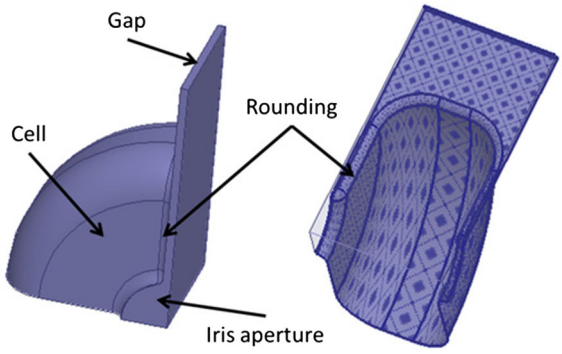


FIG. 2. HFSS model of a single cell quarter, a flatbed region representing gap added to house the metal joining surface [7,9].

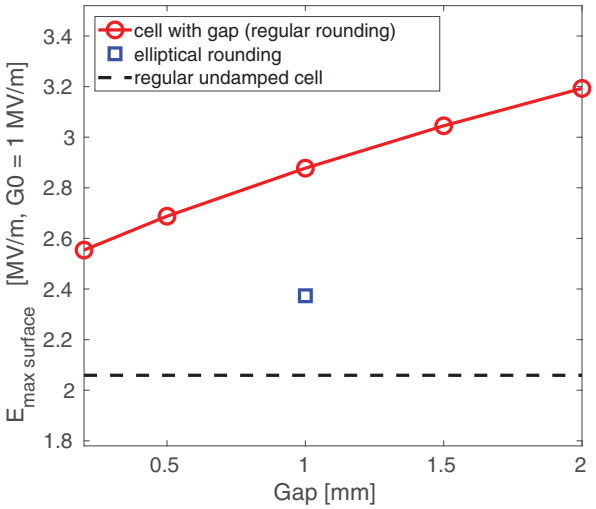


(a) Peak Surface Electric Field.

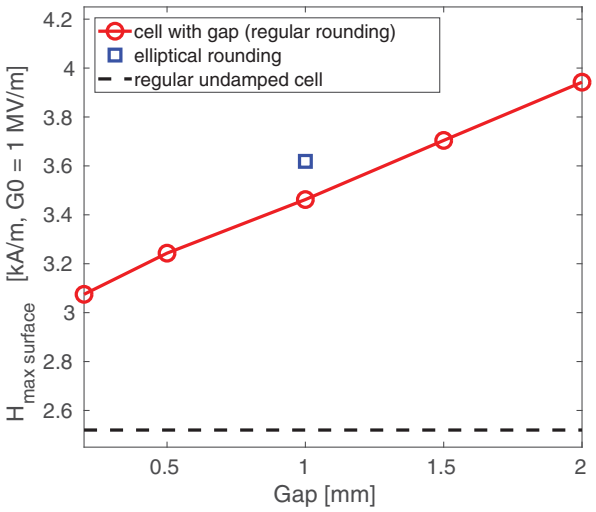


(b) Peak Surface Magnetic Field.

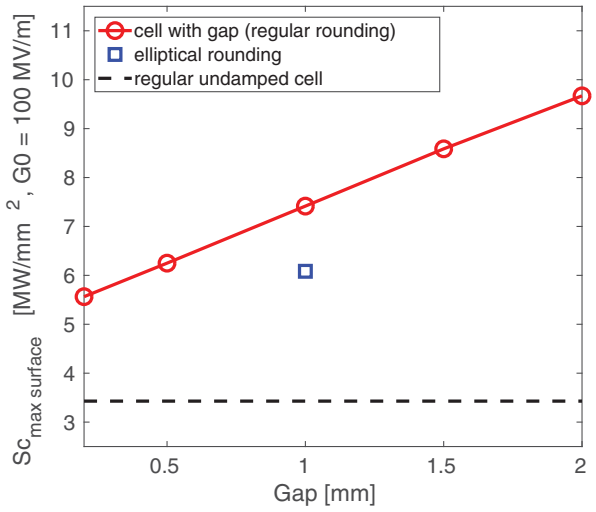


(c) Peak Surface $S_c$.

FIG. 3. Surface field simulations for the CLIC-G-OPEN design compared to the CLIC-G structure. [9].

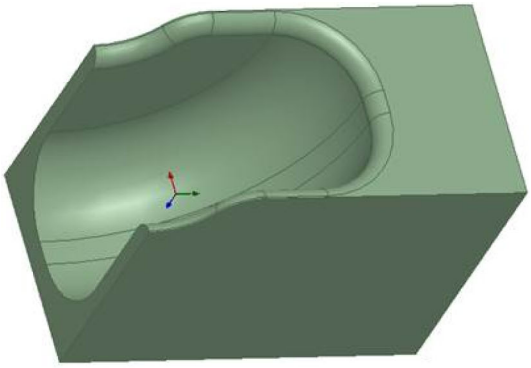

(a) Elliptical Rounding

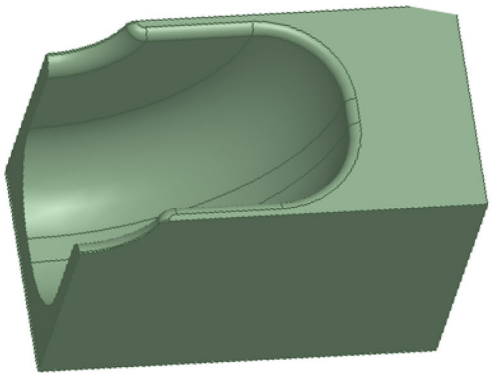

(b) Regular Rounding.

FIG. 4. Rounding profile used on the CLIC-G-OPEN compared to previous CLIC structures [7].

rf performance. We note that a similar approach could be used to reduce trapping of long-range wakefields in the structure [6]. We determined the optimal gap size and other parameters using Ansys' HFSS to model a quarter cell [7], shown in Fig. 2. The addition of this gap into a closed geometry was expected to increase surface fields. A simulation of the surface fields for various gap widths, featured in Fig. 3, indicated that a greater gap size led to

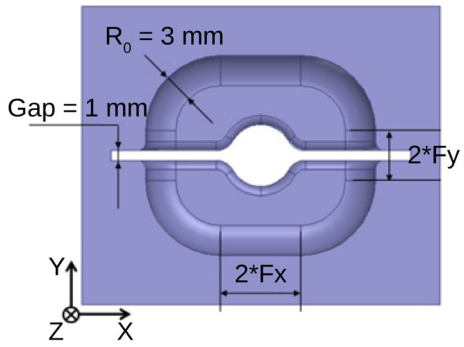


FIG. 5. A cross section of the cell geometry with parameters $F_x$ and $F_y$ which represent size of the flat region of the racetrack design [9].

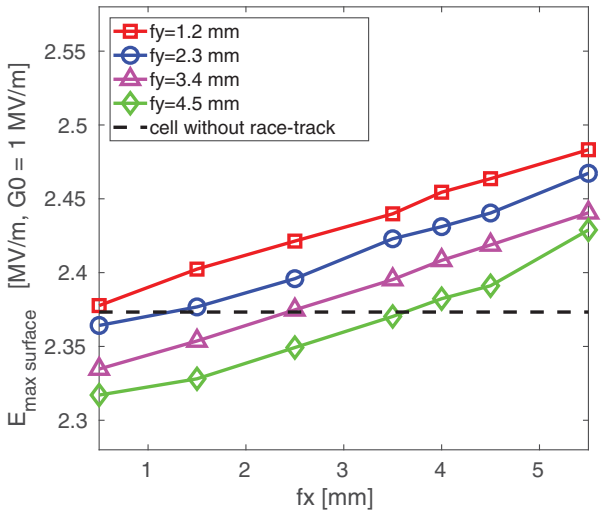


(a) Peak Surface Electric Field.

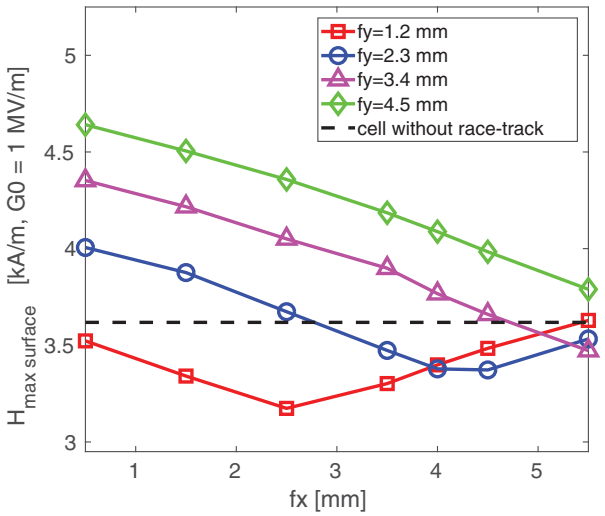


(b) Peak Surface Magnetic Field.

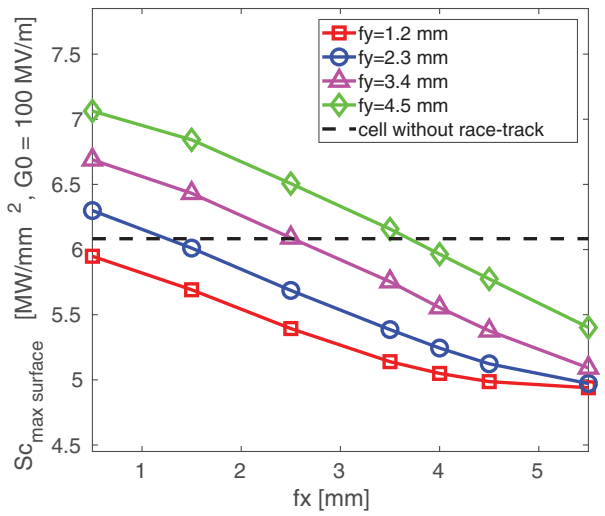


(c) Peak Surface $S_c$.

FIG. 6. Optimization of the straight sections, $F_x$ and $F_y$, in the racetrack geometry. [9].

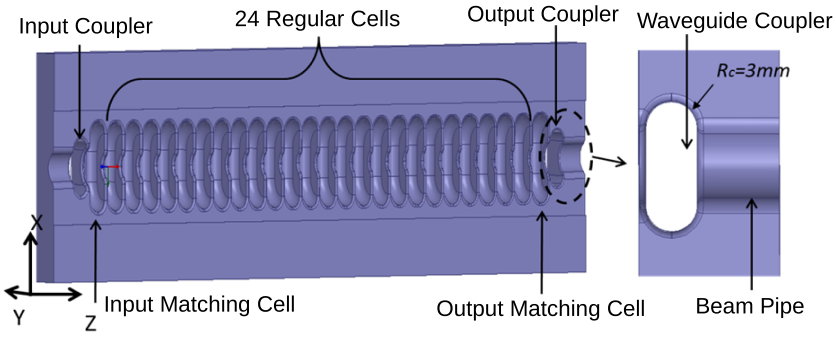


FIG. 7. CLIC-G-OPEN structure half with 24 regular cells and 2 matching cells. The waveguide coupler is also displayed on the right [11].

an increase in peak electric ($E$) and magnetic ($H$) fields, and modified Poynting vector ($S_c$). $S_c$ is closely related to local power flow [8] which is one of the main field quantities which is minimized, along with the surface electric and magnetic fields, during the design and optimization of high-gradient structures.

Figure 6 in [10] depicts a copper pulse heating sample with damage due from the exposure to extremely high electromagnetic fields. During the high power test, the sample was a part of the cavity as show in Fig. 4 in [10]. In this particular experiment, there was a gap between the sample and the cavity body approximately 25 microns wide. Since the mode in the cavity is of type TE, it was expected that there would be no field in the gap, and therefore no damage beyond radius of 2.5 cm. As seen on Fig. 6 in [10], there is obvious damage beyond edge of the cavity in the "no field" area. In the following tests the pulse-heating cavity was re-designed to eliminate the gap. With this experience in mind, we selected the gap in CLIC-G-Open to be significantly larger than 25 microns. We use 1 mm gap as a compromise between increasing the surface fields and degrading high power performance due to the small gap.

Elliptical rounding on the edges, the profile of which is demonstrated in Fig. 4, was used to simplify the fabrication process by permitting the use of a single rounding profile for each cell. Figure 3 also compares the surface fields with (blue square) and without a new elliptical edge rounding technique at the chosen gap size. Peak surface $E$ fields and $S_c$ decreased 17.5% and 18%, respectively, under the new rounding in comparison to the regular rounding at the expense of a 4.4% increase in the maximum surface $H$ field.

The cross-sectional profile of the CLIC-G-Open structure is illustrated in Fig. 5. The lengths of the horizontal and vertical flat sections are defined as $F_x$ and $F_y$, respectively. Optimization of the peak surface fields, for various values of $F_x$ and $F_y$ are depicted in Fig. 6. It can be seen that to minimize the peak $S_c$ one can increase $F_x$ and decrease $F_y$, and consequently also reduces the peak $H$ field. We chose the value $F_y = 1.2$ mm as this minimizes the peak $H$ field and $S_c$. $F_x$ was chosen to be 4.0 mm as a compromise between the peak $H$ fields and $S_c$.

## III. FULL STRUCTURE GEOMETRY

A tapered structure with 24 regular cells, 2 matching cells and waveguide couplers was generated from the optimized single cell geometry. Figure 7 demonstrates the HFSS design of the structure half and the waveguide coupler. Waveguide couplers on the CLIC-G-Open are double fed and manufactured through precision milling, with internal edges possessing a 3 mm rounding. A comprehensive list of the structure parameters is detailed in Table I together with the parameters of the undamped CLIC-G structure used as the basis for the design [11].

## IV. STRUCTURE FABRICATION AND TUNING

A prototype of the CLIC-G-Open design was fabricated at SLAC using precision milling on copper blocks. A full structure, as well as a single structure half, was produced and is seen in Fig. 8. In preparation for the brazing the rf

TABLE I. Structure parameters for the CLIC-G-Open structure compared to the CLIC-G structure [11]. All values are normalised to an unloaded gradient of 100 MV/m.

| Parameter | CLIC-G Open | CLIC-G |
|---|---|---|
| Unloaded Gradient [MV/m] | 100 | 100 |
| Input/output iris radii [mm] | 3.15/2.35 | 3.15/2.35 |
| Group velocity normalized to the speed of light (c) [%$c$] | 1.99/1.06 | 1.79/0.91 |
| Shunt impendence [MΩ/m] | 107/137 | 116/150 |
| Peak input power [MW] | 44.5 | 37.5 |
| Filling time [ns] | 49 | 57 |
| Maximum E-field [MV/m] | 268 | 222 |
| Maximum $S_c$ [MW/mm$^2$] | 5.16 | 3.51 |
| Maximum pulsed surface heating for a 200 ns pulse [K] | 25 | 14 |

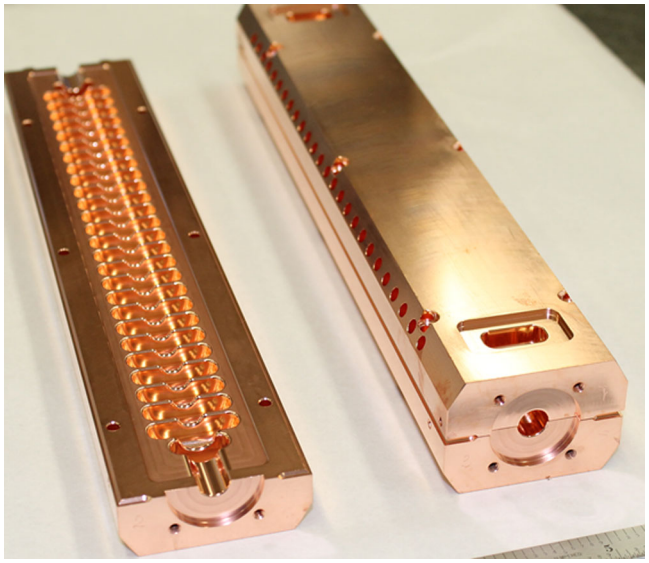

FIG. 8. Photos of the CLIC-G-OPEN after milling and after installation [11].

flanges were plated in copper and chemical etching for 30 sec removed undesirable surface structures. After cleaning, a pre-brazing beadpull measurement was performed to verify structure's dimensions. The pre-brazing beadpull was enabled by the structure design. As no rf currents flow through the joint, the rf parameters of the halves clamped are very similar to that of the brazed structure. This is not possible with the structure made from disks. Finally, atmospheric pressure hydrogen brazing adhered the two halves using a Cu-Au alloy brazing filler.

After brazing, the structure was tuned using nonresonant bead-pulling technique [12]. A comparison of the S-parameters for the brazed structure before and after tuning, as well as the results from the bead-pull measurements, are exhibited in Fig. 9. A good field flatness and low phase advance spread of $120° \pm 2°$ was achieved after tuning. Ultimately, the structure was fired in an ultra-high vacuum at 550°C for over eight hours to asymptote the pressure at temperature.

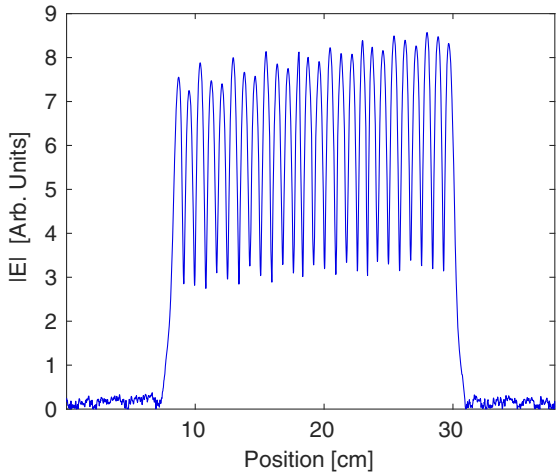


(a) On-axis electric field amplitude.

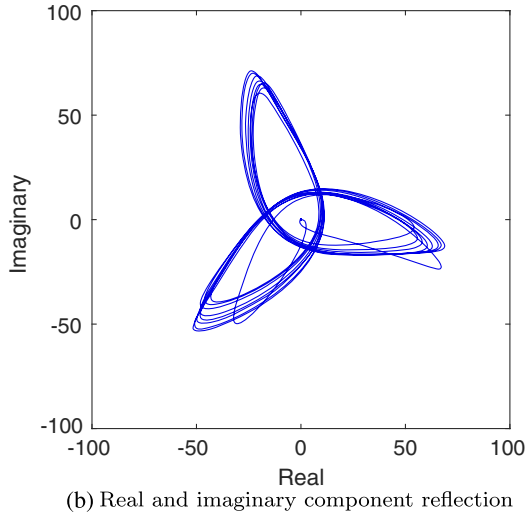


(b) Real and imaginary component reflection from bead-pull measurements.

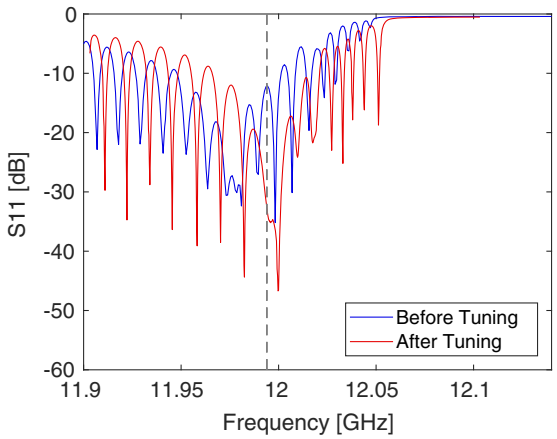


(c) S11 input from coupler as brazed and final.

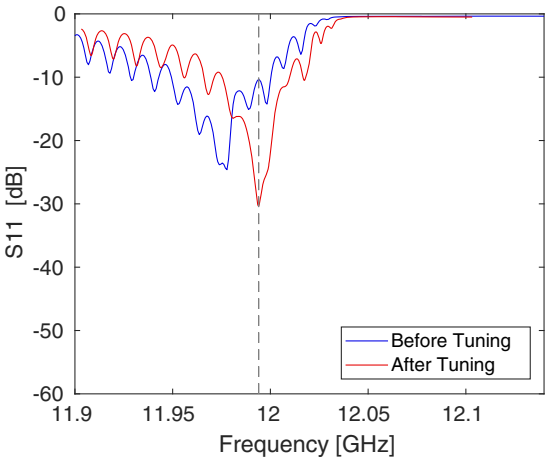


(d) S11 from output coupler as brazed and final.

FIG. 9. S-parameters and results from bead-pull measurement of the brazed structure before and after tuning [11].

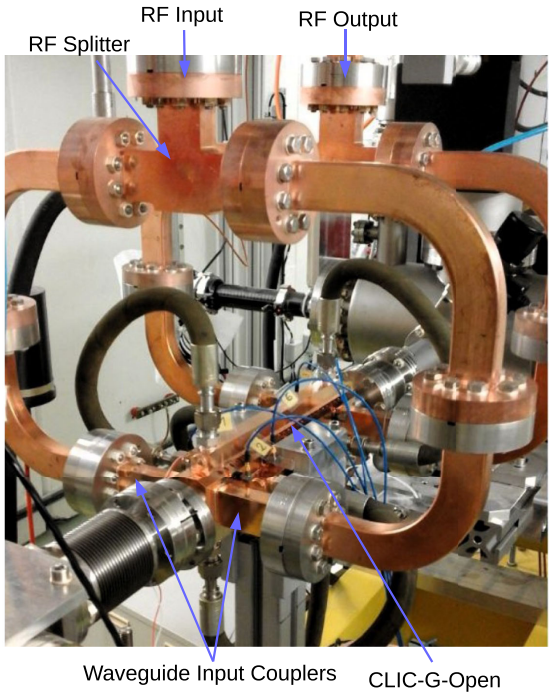


FIG. 10. Photos of the CLIC-G-OPEN after milling and after installation [11].

## V. HIGH POWER TESTING

Following tuning, the structure was shipped to CERN where high power testing was conducted on the Xbox-2 X-band test stand (Fig. 10). First commissioned in 2012, Xbox-2 is the second X-band test stand at CERN. The CLIC-G-Open structure was the second structure conditioned at this test stand following a crab cavity test [13]. Based on the same high power infrastructure as Xbox-1 [14], Xbox-2 uses a 50 MW CPI

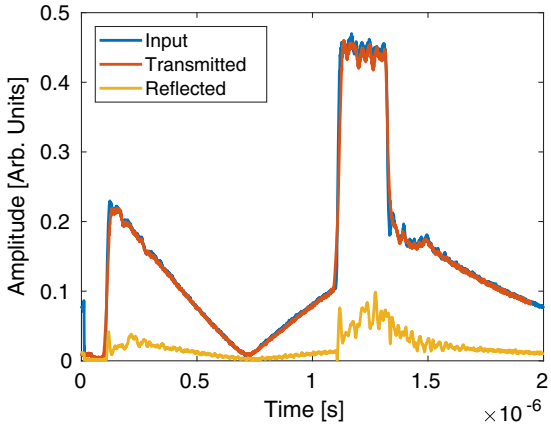


(a) Normal Pulse

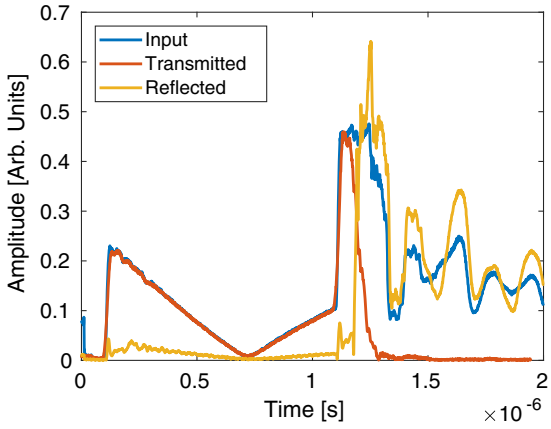


(b) Breakdown Pulse

FIG. 11. Example of the rf signals for the input, transmitted, and reflected signals.

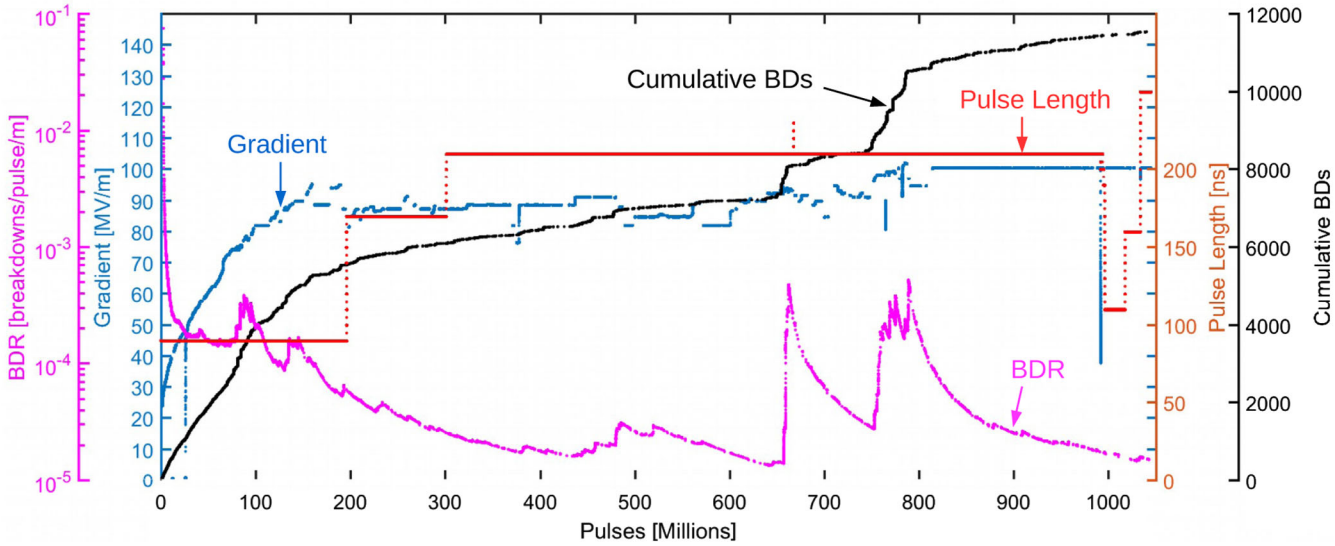


FIG. 12. Summary of the CLIC-G-Open high power test history.

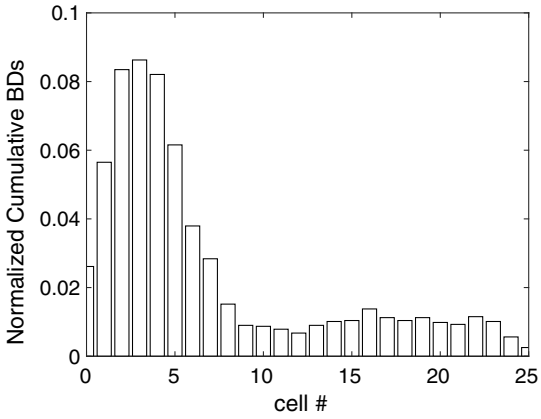


(a) Breakdown distribution along the structure.

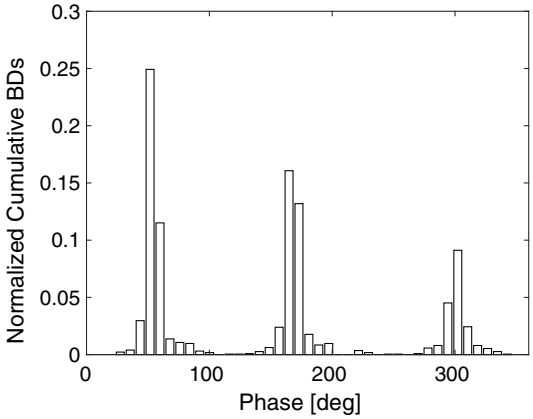


(b) Phase differential from input to reflected RF signals.

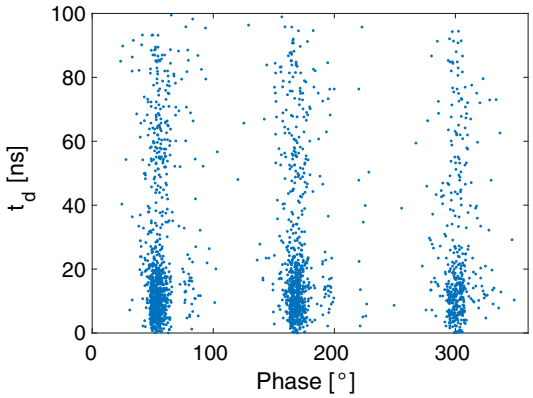


(c) Breakdown distribution along the structure vs phase differential from input and reflect RF signal. Grid lines demonstrate the cell boundaries.

FIG. 13. Breakdown distributions inside the structure normalized to the total number of breakdowns.

klystron and Scandinova modulator with a maximum pulse length of 1.5 $\mu$s operating at 50 Hz. Further amplification was achieved through the use of a SLED-I pulse compressor. The pulse compressor can be fully detuned using mechanical pistons for instances where the additional amplification is not required.

For diagnostics of the rf signals, 50 dB directional couplers installed on the waveguide network at the input and output of the structure allow for the measurement of the incident, transmitted, and reflected rf signals from the structure. These signals, along with DC signals from two Faraday cups placed upstream and downstream, were used for breakdown diagnostics, including breakdown location. Understanding the distribution of breakdowns within the structure is key to understanding the performance of a structure and the limiting factors in its design. A time-of-propagation method is used to find the location of a breakdown using the rising edge of the reflected signal and falling edge of the transmitted signal. Figure 11 displays an example of an rf pulse with and without a breakdown. The real-time system used a threshold detector on the rf and DC signals to trigger during a breakdown event, logging the breakdown event and two pulses before the breakdown as reference signals. Controlling the conditioning of the structure was an algorithm originally written for Xbox-1 in 2013 [14–16]. Pulsing began in September of 2015 and by the end of high power testing the structure had undergone 1.05 billion pulses and 11 700 breakdowns. Figure 12 summarizes the history of the structure's high power testing. At the beginning of the conditioning process, the breakdown rate (magenta) was kept at a constant $2.5 \times 10^{-4}$ breakdowns/pulse/m. Once reaching an unloaded gradient of 95 MV/m (blue) at 150 million pulses, radiation emitted from the structure exceeded the maximum safety limit outside the bunker. As the input power to the structure could not be increased until this issue was solved, the structure ran at a reduced and constant gradient of 90 MV/m. This began at 150 million pulses with the first pulse length of 90 ns where the structure continued to condition, demonstrated by the decreasing trend in the breakdown rate seen up to 200 million pulses. Conditioning of the structure led to a reduction in radiation and allowed the pulse length to be increased, without surpassing the maximum radiation safety limit, firstly to 160 ns at 200 million pulses. From 300 million pulses onwards the final pulse length of 200 ns was set. Various experiments were performed investigating the relation between power and BDR, seen as steps in the power. Increased shielding on the bunker, applied after 600 million pulses, allowed the resumption of power increments towards 100 MV/m. Once reaching the desired 100 MV/m, at 800 million pulses, the structure ran with constant gradient and conditioned down to a low breakdown rate. At 1.05 billion pulses, a breakdown rate of $< 1.5 \times 10^{-5}$ breakdowns/pulse/m was achieved at which time the structure conditioning

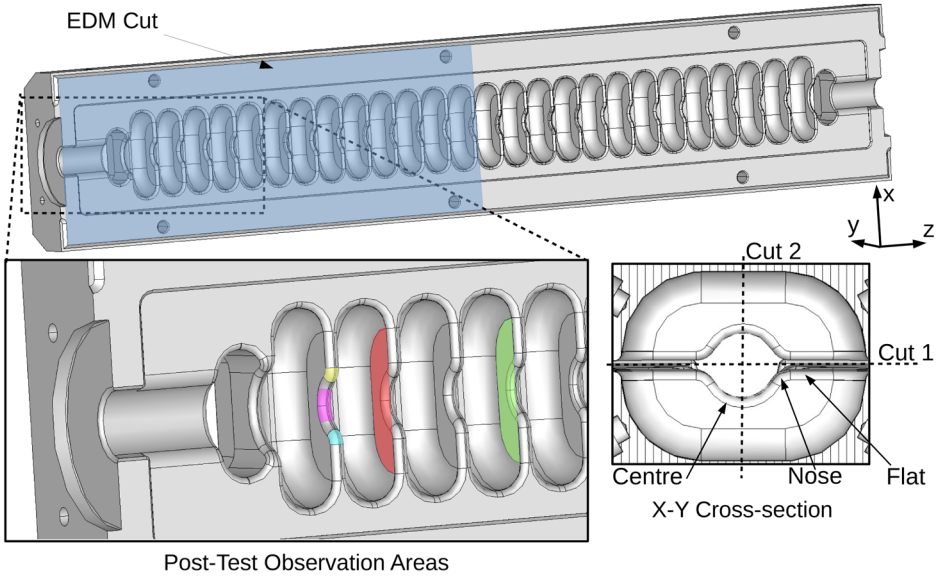


FIG. 14. Diagram of a half of the CLIC-G-OPEN structure demonstrating the EDM cut in blue. Post-test observations with a borescope looked at the iris 2 (red) and iris 4 (green) before cutting. After cutting, SEM images of the first iris looked at the left (yellow) and right (cyan) nose, and the center (magenta). An X-Y cross section demonstrating structure nomenclature.

was concluded. The achieved gradient of 100 MV/m with a 200 ns pulse is comparable to the gradient achieved by other structures up to this time, demonstrating the validity of the fabrication technique.

After conditioning, the breakdown distributions were analyzed to understand the limiting factors of the design [17]. Figure 13(a) displays the breakdown distribution in the CLIC-G-Open after conditioning, translated into a cell number and normalized to the total number of breakdowns. Breakdowns occurred predominantly toward the input of the structure.

Measuring the phase of the incident and reflected rf signals gives breakdown location information due to the known phase advance per cell. For CLIC structures, the phase advance is 120° per cell which means that the breakdowns can be diagnosed to location within a 3 cell segment which repeats throughout the structure as the phase wraps upon itself. Figure 13(b) demonstrates that the breakdown distribution appeared as three peaks for the measured phase difference.

Plotting the phase difference against the positional distribution, Fig. 13(c) illustrates a structure predominantly undergoing rf breakdown in a few adjacent irises at the input of the structure. Understanding this nonuniform breakdown distribution is key to improving the next iteration of a structure designed from halves.

## VI. POST-TEST SURFACE EXAMINATION

After removing the structure from Xbox-2, the structure was stored as a radioactive material for several months remaining in a nitrogen environment to prevent surface degradation. Figure 14 describes the structure's nomenclature and areas surveyed in the post-test analysis. To begin, S-parameter and bead-pull measurements were performed to evaluate the change in rf properties due to the high power testing. In contrast to most other high gradient structures, the investigated CLIC-G-Open demonstrated nearly no change in the electric field distribution (amplitude and phase advance per cell) and only slight changes in the S-parameters for the input and output coupler, see Fig. 15.

Before the structure underwent cutting, a borescope was used to observe any visible physical damage. Pictures from the borescope signified that the breakdown induced damage was towards the start of the structure (Fig. 16). For closer examination the structure was cut using electron discharge machining (EDM) and divided into several sections; two halves cut through the brazing material (Cut 1) for cells 1 to 13, two halves for cells 14 to 19 (Cut 2), and the rest of the structure remained intact.

A photo of the half section containing cells 1 to 13 is displayed in Fig. 17. Marked in a blue box is an issue which came to light after the structure was cut. During the brazing procedure, brazing alloy leaked from the joint into the rf region of the structure. This material reached within 200 $\mu$m of the cell edge. To determine the effect of the leak on the structure performance the halves were observed with a scanning electron microscope (SEM). Images of the surface, seen in Fig. 18, demonstrate the breakdown density on the center and nose sections of the cell. Breakdowns occurred primarily on the nose section with only a few visible marks on the center section. Overlaying the surface $E$ field and $S_c$ we find that the breakdowns are most likely

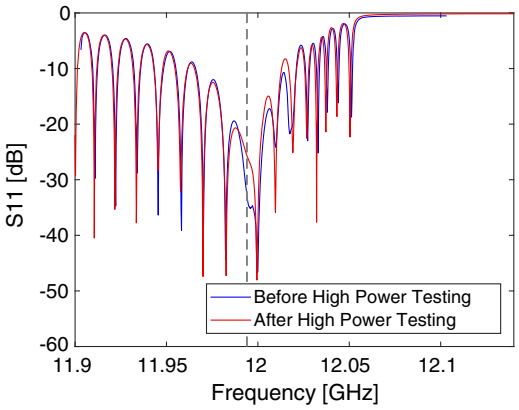


(a) S11 from input coupler.

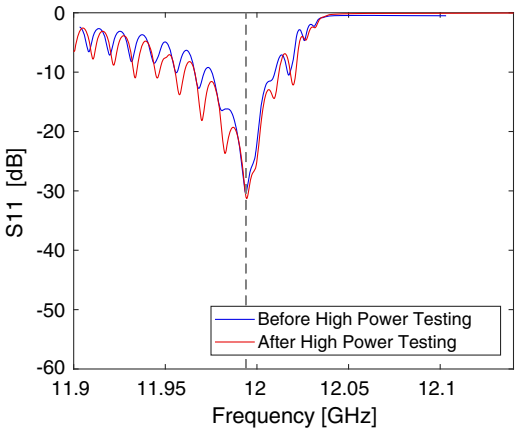


(b) S11 from output coupler.

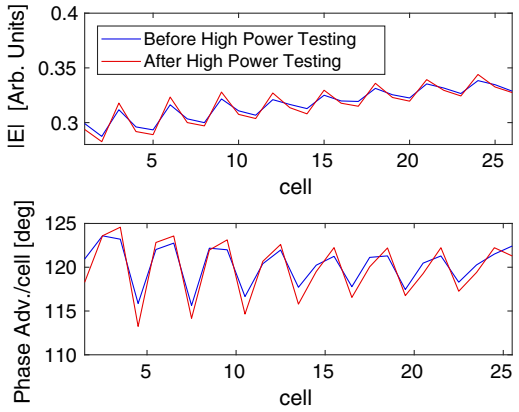


(c) Electric field amplitude and phase distributions.

FIG. 15. A comparison of the rf tests before and after high power testing.

to occur around the area with the greatest $E$ or $S_c$ though due to the similarities on the field profiles we are unable to distinguish which was the cause. Comparing the breakdown densities of the two opposing nose sections demonstrated similar numbers for the two sided. Given this, we found that the breakdowns preference for the first few cells was not related to the brazing filler leak.

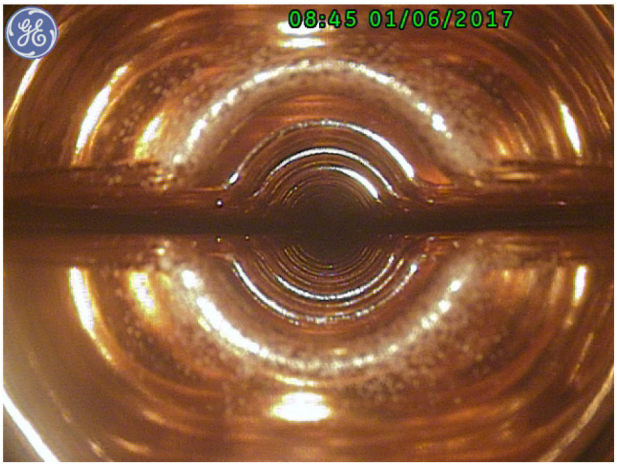


(a) Iris 2


(b) Iris 4

FIG. 16. Borescope images from the structure after conditioning. The location of the irises is described in Fig. 14.

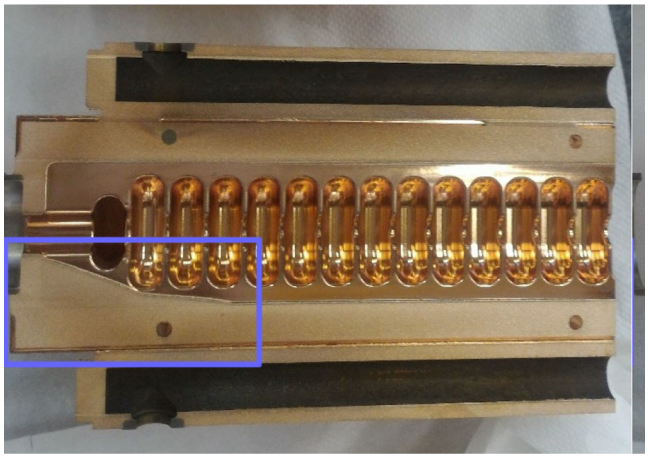

FIG. 17. Leaked brazing material visible at the input of the structure circled in blue.

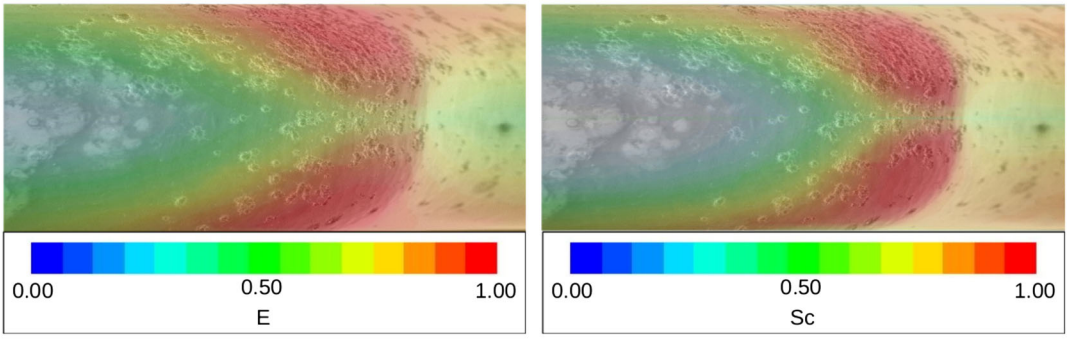


(a) $E$ on Nose Left. (b) $S_c$ on Nose Left.

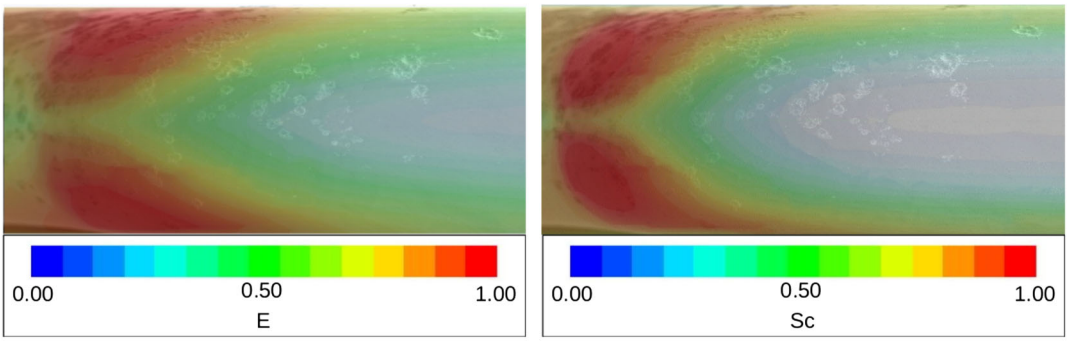


(c) $E$ on nose right. (d) $S_c$ on nose right.

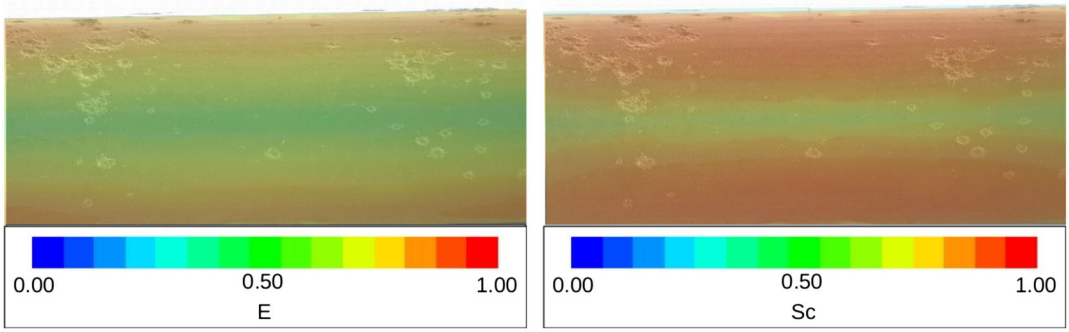


(e) $E$ on centre. (f) $S_c$ on centre.

FIG. 18. Scanning electron microscope images of various segments along the first iris. Overlaid is a field map of the surface electric field for a comparison of the breakdown location to the field strength. The location of each scan is described in Fig. 14.

## VII. CONCLUSION

A prototype for an 11.994 GHz CLIC structure made through a novel fabrication technique has been designed, fabricated and tested in a collaborative effort between CERN and SLAC. With the aim of a more cost-effective fabrication, the structure is designed to be manufactured from two milled halves and brazed together. Testing of the structure at high power was performed at CERN's Xbox-2 where the structure underwent high power testing for 1.05 billion pulses. Ultimately an unloaded gradient of 100 MV/m at a BDR of $1.5 \times 10^{-5}$ breakdowns/pulse/m was achieved with a 200 ns pulse which is comparable to other CLIC structures. Breakdown distributions were found from analyzing the waveforms during testing. These distributions demonstrated a dominance of breakdowns towards the start of the structure which was confirmed with a post-test analysis. Post-test rf measurements demonstrated that the rf properties were very similar before and after high power testing. Observations of the structure found brazing filler leaked around the input cells of the structure though it was determined that this did not affect the breakdown distribution. The next generation of the CLIC-G-OPEN is being built. This structure will have identical rf geometry but be made from a hard CuAg alloy and joined using electron beam welding. The choice of a hard copper alloy results from extensive testing which has demonstrated that hard copper performs better at high gradients than soft copper [10,18].

## ACKNOWLEDGMENTS

The authors would like to sincerely thank the structure production teams at CERN and SLAC for their essential contributions to the preparations and follow up of this experiment.

[1] M. Aicheler *et al.*, A Multi-TeV Linear Collider Based on CLIC Technology, Repotr No. CERN 2012-007.

[2] J. W. Wang, J. R. Lewandowski, J. W. Van Pelt, C. Yoneda, G. Riddone *et al.*, Fabrication technologies of the high gradient accelerator structures at 100 MV/m range, in *Proceedings of the International Particle Accelerator Conference, Kyoto, Japan* (ICR, Kyoto, 2010).

[3] T. Abe, Y. Arakida, T. Higo *et al.*, Basic Study on high gradient accelerating structure at KEK/NEXTEF, *12th Annual Meeting of Particle Accelerator Society of Japan*, http://www.pasj.jp/web_publish/pasj2015/proceedings/index.html.

[4] A. Solodko, X-band accelerating structure fabrication in the perspective of mass production and cost optimization, Talk at LCWS 2017, 2017, Strasbourg (unpublished).

[5] B. Woolley, *High Power X-band RF Test Stand Development and High Power Testing of the CLIC Crab Cavity*, Lancaster University, United Kingdom (Lancaster University, 2015).

[6] S. Doebert *et al.*, High power test of an X-band slotted iris acccelerating structure at NLCTA, in *Proceedings of the 22nd Particle Accelerator Conference, PAC-2007, Albuquerque, NM* (IEEE, New York, 2007).

[7] Ansys HFSS, http://www.ansys.com.

[8] A. Grudiev, S. Calatroni, and W. Wuensch, New local field quantity describing the high gradient limit of accelerating structures, Phys. Rev. ST Accel. Beams **12**, 102001 (2009).

[9] H. Zha, A. Grudiev, and V. Dolgashev, RF Design of the CLIC structure prototype optimized for manufacturing from two halves, IPAC15, Richmond, USA, in *Proceedings of the 6th International Particle Accelerator Conference* (Jacow, Richmond, 2015).

[10] L. Laurent, S. Tantawi, V. Dolgashev, C. Nantista, Y. Higashi, M. Aicheler, S. Heikkinen, and W. Wuensch, Experimental study of rf pulse heating, Phys. Rev. ST Accel. Beams **14**, 041001 (2011).

[11] N. Catalan *et al.*, Fabrication and high gradient testing of an accelerating structure made from milled halves, in *Proceedings of the 28th Linear Accelerator Conference* (Jacow, East Lansing, 2016).

[12] C. W. Steele, A non-resonant perturbation theory, IEEE Trans. Microwave Theory Tech. **14**, 70 (1966).

[13] B. Woolley *et al.*, High gradient testing of an X-band crab cavity at XBOX2, IPAC15, Richmond, USA, in *Proceedings of the 6th International Particle Accelerator Conference* (Jacow, Richmond, 2015).

[14] N. Catalan-Lasheras *et al.*, Experiences operating an X-band high-power test stand at CERN, IPAC14, Dresden, Germany, in *Proceedings of the 5th International Particle Accelerator Conference* (Jacow, Dresden, 2014).

[15] National Instruments, http://www.ni.com.

[16] A. Degiovanni *et al.*, High-gradient test results from a CLIC prototype accelerating structure: TD26CC, IPAC14, Dresden, Germany, in *Proceedings of the 5th International Particle Accelerator Conference* (Jacow, Dresden, 2014).

[17] A. Degiovanni *et al.*, Diagnostics and analysis techniques for high power X-band accelerating structures, LINAC14, Geneva, Switzerland, in (Jacow, Geneva, 2014).

[18] E. I. Simakov *et al.*, Advances in high gradient normal conducting accelerator structures, Nucl. Instrum. Methods Phys. Res., Sect. A, DOI: 10.1016/j.nima.2018.02.085 (2018).